



THE UNIVERSITY *of* EDINBURGH

## Edinburgh Research Explorer

# Modeling of laser generation in a Fabry–Pérot-Tamm structure with a nematic liquid crystal layer

### Citation for published version:

Yakovkin, I, Ledney, M, Reshetnyak, V, Pakamoryte, I & Hands, PJW 2024, 'Modeling of laser generation in a Fabry–Pérot-Tamm structure with a nematic liquid crystal layer', *Journal of applied physics*, vol. 135, no. 21, 213102. <https://doi.org/10.1063/5.0208565>

### Digital Object Identifier (DOI):

[10.1063/5.0208565](https://doi.org/10.1063/5.0208565)

### Link:

[Link to publication record in Edinburgh Research Explorer](#)

### Document Version:

Publisher's PDF, also known as Version of record

### Published In:

Journal of applied physics

### General rights

Copyright for the publications made accessible via the Edinburgh Research Explorer is retained by the author(s) and / or other copyright owners and it is a condition of accessing these publications that users recognise and abide by the legal requirements associated with these rights.







### Take down policy

The University of Edinburgh has made every reasonable effort to ensure that Edinburgh Research Explorer content complies with UK legislation. If you believe that the public display of this file breaches copyright please contact [openaccess@ed.ac.uk](mailto:openaccess@ed.ac.uk) providing details, and we will remove access to the work immediately and investigate your claim.



RESEARCH ARTICLE | JUNE 05 2024

## Modeling of laser generation in a Fabry–Pérot–Tamm structure with a nematic liquid crystal layer

I. I. Yakovkin ; M. F. Ledney ; V. Yu. Reshetnyak ; I. Pakamoryte ; P. J. W. Hands  



*J. Appl. Phys.* 135, 213102 (2024)

<https://doi.org/10.1063/5.0208565>



Journal of Applied Physics

Publish open access for free

[Learn More](#)



# Modeling of laser generation in a Fabry-Pérot-Tamm structure with a nematic liquid crystal layer

Cite as: J. Appl. Phys. 135, 213102 (2024); doi: 10.1063/5.0208565

Submitted: 15 March 2024 · Accepted: 15 May 2024 ·

Published Online: 5 June 2024



I. I. Yakovkin,<sup>1</sup> M. F. Ledney,<sup>1</sup> V. Yu. Reshetnyak,<sup>2</sup> I. Pakamoryte,<sup>3</sup> and P. J. W. Hands<sup>3,a)</sup>

## AFFILIATIONS

<sup>1</sup>Physics Faculty, Taras Shevchenko National University of Kyiv, Kyiv, Ukraine

<sup>2</sup>School of Physics and Astronomy, University of Leeds, Leeds, United Kingdom

<sup>3</sup>School of Engineering, Institute for Integrated Micro and Nano Systems, University of Edinburgh, Edinburgh, United Kingdom

**Note:** This paper is part of the special topic, Plasmonics and Optical Metastructures.

**a) Author to whom correspondence should be addressed:** philip.hands@ed.ac.uk

## ABSTRACT

In the presented work, the possibility of controlling laser generation using a nematic liquid crystal (NLC) in a hybrid layered structure consisting of a thin metal layer (Ag), a layer of NLC doped with a light-absorbing dye, and a distributed Bragg reflector (DBR) with a rectangular refractive index profile is theoretically studied. Spectral dependencies of the reflection, transmission, and absorption coefficients of light as well as the localization coefficient of the light field in NLC within the photonic bandgap of the DBR are obtained. Narrow dips in the reflection coefficient and peaks in the transmission coefficient are achieved due to the excitation of plasmons at the Ag-NLC interface. The dependence of the spectral position and magnitude of the plasmonic dips/peaks and the enhancement of the light field in the NLC medium on the thickness and orientation of the NLC layer as well as the impact of a light-absorbing dye doping are investigated. Theoretical calculations of the temporal dependencies of luminescence pulses for pumping pulses of different power settings (below, above, and at the threshold of laser generation) and different values of light absorption in the dye-doped NLC medium are performed, taking into account the peculiarities of the optical properties of the dye-doped NLC.

© 2024 Author(s). All article content, except where otherwise noted, is licensed under a Creative Commons Attribution (CC BY) license (<https://creativecommons.org/licenses/by/4.0/>). <https://doi.org/10.1063/5.0208565>

## I. INTRODUCTION

Over the past few decades, localized electromagnetic modes occurring at the interface between a metal and a distributed Bragg reflector (DBR) with a rectangular refractive index profile have attracted increased attention. These electromagnetic modes are known as Tamm plasmon polaritons (TPPs).<sup>1–8</sup> TPPs owe their existence to the combination of the metal's negative dielectric permittivity and the presence of a photonic bandgap in the Bragg reflector. Unlike ordinary surface plasmon polaritons,<sup>9–17</sup> the excitation of TPPs does not require the presence of a prism or a periodic grating. In experiments, TPPs manifest as narrow dips/peaks in the optical reflection/transmission spectra within the photonic bandgap of the DBR. The ability of liquid crystals (LCs) to easily change their orientational ordering of the mesophase and,

consequently, their optical properties, under the influence of external electric/magnetic and light fields, temperature changes, and the addition of various additives, including fluorescent dyes, opens up broad possibilities for controlling both ordinary surface plasmons<sup>18–23</sup> and TPPs.<sup>24,25</sup> In the latter case, a controlling LC layer placed between the metal and DBR provides additional degrees of influence on TPP characteristics.<sup>26,27</sup> In several studies,<sup>28–32</sup> a cholesteric liquid crystal (CLC) was used as the distributed Bragg reflector, as it exhibits Bragg reflection of circularly polarized light if the directions of light polarization and the helix axis of the cholesteric spiral coincide. To improve the optical characteristics of TPPs and provide additional degrees of influence on them, the use of rugate filters (RFs)<sup>33–37</sup> with a smooth periodic refractive index profile was proposed instead of DBRs with a

05 June 2024 19:19:54

rectangular profile. The possibilities for controlling the characteristics of TPPs open up potential applications of TPPs in sensors,<sup>38–42</sup> optical switches and filters,<sup>43–45</sup> as well as in selective thermal and light emitters.<sup>46–48</sup> It should be noted that Tamm-plasmonic structures, characterized by the confinement of electromagnetic modes at the interface of a photonic crystal and metal, are also promising platforms for laser generation due to the possibility of local enhancement of the electromagnetic field.<sup>49–53</sup>

LCs are widely used in lasers to provide cost-effective and tunable solutions for modern photonic applications. The reorientation of LCs by the influence of external factors allows for changes in the resonant properties of the lasing cavity, typically formed by metal, dielectric, or distributed Bragg reflectors. This enables dynamic tunability of the lasing polarization and wavelength, unmatched by typical semiconductor or gas lasers. Such adaptability is achieved through external fields,<sup>54,55</sup> temperature adjustments,<sup>56,57</sup> or mechanical stress,<sup>58</sup> with nematic liquid crystals (NLCs) being particularly effective for dynamically tuning laser output within a Fabry–Pérot cavity, as demonstrated in Refs. 59 and 60. The range of laser wavelength tuning can vary significantly, with electro-induced reorientation of the NLC director allowing for changes of up to 30 nm,<sup>61</sup> while thermo-optical tuning offers a more modest shift of 2–3 nm.<sup>62</sup> Precision control of the laser wavelength to within 0.008 nm via NLC reorientation has been explored in Ref. 63, illustrating the sophisticated capability of LC lasers in photonics.

LCs doped with fluorescent dyes can act as an active medium for lasers.<sup>64</sup> Dye-doped CLCs, with their inherent one-dimensional photonic crystal structure, are widely used to enhance lasing<sup>31,65–68</sup> and to enable remarkable tunability beyond 300 nm.<sup>32</sup> The use of dye-doped NLCs within lasing systems based on distributed feedback<sup>69</sup> has also proven to be a promising way of achieving dynamic tunability.<sup>70</sup>

In the presented work, the possibility of controlling laser generation in a Tamm-plasmon hybrid metal-NLC-DBR structure using a dye-doped nematic liquid crystal (NLC) is theoretically investigated. The paper is structured as follows. Section II describes the model of the structure and presents equations for calculating the light reflection and transmission coefficients within the DBR bandgap region near the Bragg resonance condition. Section III presents the results of numerical calculations of the spectral dependencies of the reflection, transmission, absorption coefficients, and light field enhancement factor in the NLC medium. The effects of the thickness and orientation of the NLC layer and the presence of light absorption in the NLC volume on these quantities are analyzed. In Sec. IV, using rate equations, the temporal dependencies of luminescence pulses for different powers (below, at, and above the threshold of laser generation) of the pumping pulse are theoretically calculated. The discussion of the results and brief conclusions are presented in Sec. V.

## II. STRUCTURE MODEL AND THEORY

The structure under consideration consists of an NLC placed between a metal film and a DBR. The orientation of the NLC's director is assumed to be homeotropic and uniform, meaning that the director throughout the NLC volume is oriented perpendicular

to the layers bounding this volume. The DBR is formed by alternating two homogeneous dielectric layers, resulting in a rectangular refractive index profile of the DBR medium. On the opposite side, the DBR layer is bounded by a homogeneous dielectric substrate. A plane monochromatic light wave of frequency  $\omega$ , polarized in the direction of the  $x$ -axis, oriented along the interface of the NLC and DBR, propagates normally toward the metal film from the air in the positive direction of the  $z$ -axis. The light wave, after passing through the metal film, enters the NLC layer and subsequently into the DBR medium and dielectric substrate, undergoing a series of successive reflections at the interfaces of the layers. The scheme of the structure under consideration, along with the directions of the incident ( $A_i$ ) and reflected ( $B_i$ ) electromagnetic waves, is presented in Fig. 1. It is necessary to admit that the proposed structure may be impractical to fabricate, as it currently requires a floating metal layer on top of the NLC. Future modeling work might, therefore, include the possibilities for addition of a supporting substrate either above or below the metal layer. However, this has not been included here for the purpose of simplifying the model while still demonstrating the principles of lasing within Tamm-plasmonic NLC structures. It should be noted that the presence of a metal layer leads to increased absorption of electromagnetic waves. However, the use of the mirror structures composed of two planar layers of indium tin oxide (ITO mirrors) and metallic mirrors simplifies the production process and lowers the costs, which is important to make NLC lasers competitive with common CLC lasers.<sup>71</sup>

In each layer of the considered structure, the electric field intensity vector  $\vec{E}_i$  of the light wave is a solution of the wave

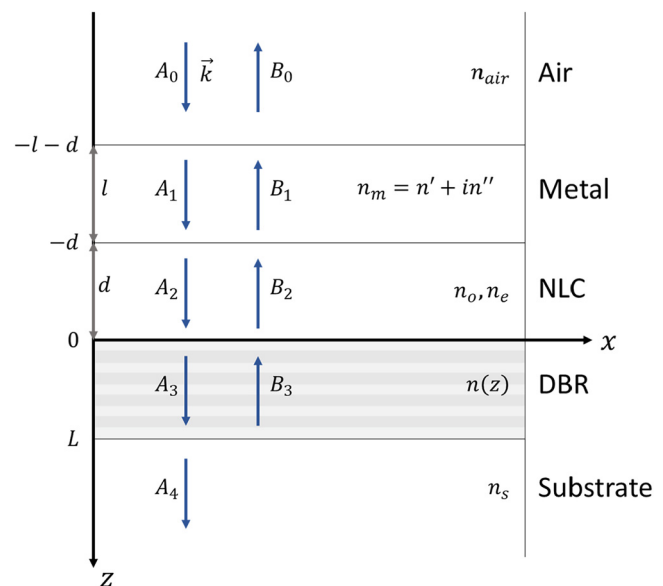


FIG. 1. Tamm-plasmonic structure of metal film-NLC-DBR under study. The pump wave is propagating along the  $z$  direction, and the wave amplitudes in each medium are denoted as  $A_i$  and  $B_i$  for forward- and backward-propagating waves, respectively.

05 June 2024 19:19:54

equation  $\Delta \vec{E}_i + \frac{\omega^2}{c^2} \varepsilon_i \vec{E}_i = 0$ , where  $\varepsilon_i$  is the dielectric permittivity of the respective layer. The magnetic field strength vector  $\vec{H}_i$  is found from Maxwell's equation  $\text{rot } \vec{E}_i = -\partial \vec{B}_i / \partial t$ . In the directions of the coordinate axes  $x$  and  $y$ , the system under consideration is assumed to be homogeneous. Within each layer of the structure, the strength vectors  $\vec{E}_i$  of the electric and  $\vec{H}_i$  magnetic fields will have the form, respectively,  $\vec{E}_i = (E_i(z), 0, 0)$  and  $\vec{H}_i = (0, H_i(z), 0)$ . Accordingly, in the air at  $z \leq -l - d$ , in the metal film at  $-l - d \leq z \leq -d$ , and in the NLC layer at  $-d \leq z \leq 0$ , the electric  $E_i$  and magnetic  $H_i$  field strengths of the light wave will, respectively, have the following form:

$$\begin{aligned} E_i(z) &= A_i e^{ikn_i z} + B_i e^{-ikn_i z}, \\ H_i(z) &= \frac{n_i}{c\mu_0} (A_i e^{ikn_i z} - B_i e^{-ikn_i z}). \end{aligned} \quad (1)$$

Here,  $k = \omega/c$  represents the wavenumber of the electromagnetic wave in vacuum, with  $i = 0, 1$ , and  $2$  denoting air, metal, and NLC with refractive indices  $n_{\text{air}} = 1$ ,  $n_m = n'_m + in''_m$ , respectively, and  $n_{LC} = n_o$ —the refractive index of the ordinary wave in NLC (see Fig. 1). In Eq. (1), the intensity of the incident light wave was considered to be small enough to not change the initial uniform homeotropic orientation of the NLC director. Here, the absorption of light by the layers of the system, including the DBR layer, is considered negligible.

In the region  $0 \leq z \leq L$ , within each of the dielectric layers of the DBR structure, the vectors of the electric and magnetic field strengths of the light wave will take the form given by formula (1), where  $n_i$  is the dielectric constant of the corresponding layer of the DBR.

Below the DBR, for  $z \geq L$ , in the dielectric substrate with a refractive index  $n_s$ , only the wave that has passed through the system is present, resulting in the following vectors of the electric and magnetic field strengths:

$$\begin{aligned} E_4(z) &= A_4 e^{ikn_s z}, \\ H_4(z) &= n_s A_4 / (c\mu_0) e^{ikn_s z}. \end{aligned} \quad (2)$$

At the interfaces of the dielectric layers, the vectors of the electric field strength  $\vec{E}_i$  and the magnetic field strength  $\vec{H}_i$  of the light wave must satisfy the boundary conditions of electrodynamics. From the latter, we find the intensities of the electric field  $B_0$  of the reflected wave and  $A_4$  of the wave that has passed through the system. This allows to obtain the values of the reflection coefficient  $R = |B_0/A_0|^2$  and the transmission coefficient  $T = n_s |A_4/A_0|^2$  of the system. Even with a relatively small number of DBR dielectric layers, an analytical solution to the problem is excessively cumbersome. Therefore, it is practical to solve the problem numerically. However, in the case when the Bragg resonance condition is met in the DBR medium, an analytical description of the problem is possible. In the region  $0 \leq z \leq L$ , we decompose the dielectric permittivity of the DBR medium into the Fourier series along the coordinate  $z$  as a periodic function with period  $a$ ,

$$\varepsilon(z) = \varepsilon_0 + \sum_{j \neq 0}^{\infty} \varepsilon_j e^{i2\pi jz/a}. \quad (3)$$

We will assume that the wavelength  $\lambda$  of the incident light is close to the Bragg wavelength  $\lambda_B = 2\bar{n}a/m$ , where  $m$  is an integer and  $\bar{n} = \sqrt{\varepsilon_0}$  is the mean refractive index of the DBR medium. The solution of the wave equation in the DBR medium will be sought using the method of coupled waves.<sup>72,73</sup> The vector of the electric field strength of the electromagnetic wave can be expressed as

$$E_3(z) = A_3(z) e^{ik\bar{n}z} + B_3(z) e^{-ik\bar{n}z}. \quad (4)$$

The amplitudes of the incident  $A_3(z)$  and reflected  $B_3(z)$  waves are slowly varying functions that satisfy the Kogelnik equations,<sup>72</sup>

$$\begin{aligned} \frac{d}{dz} A_3(z) &= i\chi_m e^{-i2\delta z} B_3(z), \\ \frac{d}{dz} B_3(z) &= -i\chi_{-m} e^{i2\delta z} A_3(z), \end{aligned} \quad (5)$$

where  $\chi_{\pm m} = k\varepsilon_{\pm m}/(2\bar{n})$  and  $\delta = k\bar{n} - \pi m/a$  is the deviation from the Bragg resonance condition. In  $|\delta|a \ll 1$ ,  $|\chi_{\pm m}|a \ll 1$  approximation, the solution of the Kogelnik equations (5) takes the following form:<sup>72</sup>

$$\begin{aligned} A_3(z) &= (a_1 e^{-\gamma_m z} + a_2 e^{\gamma_m z}) e^{-i\delta z}, \\ B_3(z) &= \left( a_1 r_m e^{-\gamma_m z} + \frac{a_2 \chi_{-m}}{r_m \chi_m} e^{\gamma_m z} \right) e^{i\delta z}. \end{aligned} \quad (6)$$

Here,  $\gamma_m \approx \sqrt{\chi_m \chi_{-m} - \delta^2}$ ,  $r_m = i\chi_{-m}/(\gamma_m - i\delta)$ , and  $a_1$  and  $a_2$  denote the unknown coefficients.

Taking Eq. (6) into account, the following expression for the magnetic field strength in the DBR structure is obtained:

$$\begin{aligned} H_3(z) &= \frac{1}{\omega\mu_0} (k\bar{n} e^{ik\bar{n}z} - \chi_{-m} e^{-i(k\bar{n}-2\delta)z}) A_3(z) \\ &+ \frac{1}{\omega\mu_0} (\chi_m e^{i(k\bar{n}-2\delta)z} - k\bar{n} e^{-ik\bar{n}z}) B_3(z). \end{aligned} \quad (7)$$

The electric field strength vectors  $E_i$  and magnetic field strength vectors  $H_i$  (where  $i = \overline{0, 4}$ ) of the light wave must satisfy the following boundary conditions at  $z = -l - d$ ,  $z = -d$ ,  $z = 0$ , and  $z = L$ :

$$\begin{aligned} A_0 e^{-ik(l+d)} + B_0 e^{ik(l+d)} &= A_1 e^{-ikn_m(l+d)} + B_1 e^{ikn_m(l+d)}, \\ A_0 e^{-ik(l+d)} - B_0 e^{ik(l+d)} &= n_m (A_1 e^{-ikn_m(l+d)} - B_1 e^{ikn_m(l+d)}), \\ A_1 e^{-ikn_m d} + B_1 e^{ikn_m d} &= A_2 e^{-ikn_o d} + B_2 e^{ikn_o d}, \\ n_{\text{eff}} (A_1 e^{-ikn_m d} - B_1 e^{ikn_m d}) &= n_o (A_2 e^{-ikn_o d} - B_2 e^{ikn_o d}), \\ A_2 + B_2 &= A_3(0) + B_3(0), \\ kn_o (A_2 - B_2) &= (k\bar{n} - \chi_{-m}) A_3(0) + (\chi_m - k\bar{n}) B_3(0), \\ A_3(L) e^{ik\bar{n}L} + B_3(L) e^{-ik\bar{n}L} &= A_4 e^{ikn_s L}, \\ (k\bar{n} - \chi_{-m}) A_3(L) e^{i\delta L} + (\chi_m - k\bar{n}) B_3(L) e^{-i\delta L} &= (-1)^{mp} kn_s A_4 e^{ikn_s L}, \end{aligned} \quad (8)$$

where  $p = L/a$  is the number of periods of the DBR structure. Solving the system of equations (8) results in the expressions for the amplitudes

$$R = |(1 - n_m)b_4^- e^{ikn_m d} (b_1(b_3^- r_m + b_3^+) e^{-\tilde{\gamma}L} + b_2(b_3^+ r_m \chi_m + b_3^- \chi_{-m}) e^{\tilde{\gamma}L})|^2,$$

$$T = n_s \left| \frac{-8kn_o n_m (r_m^2 \chi_m - \chi_{-m}) (b_7^+ e^{-ik\bar{n}L} + b_7^- e^{ik\bar{n}L}) e^{-ik(l+d) - ikn_s L}}{(1 + n_m)b_4^+ e^{ikn_m d} (b_2(b_3^+ r_m \chi_m + b_3^- \chi_{-m}) e^{\tilde{\gamma}L} + b_1(b_3^- r_m + b_3^+) e^{-\tilde{\gamma}L})} \right|^2. \quad (9)$$

Here,  $\tilde{\gamma} = \gamma_m + i\delta$ ,  $\eta_m = \chi_m \chi_{-m} (r_m - 1)$ ,  $b_1 = b_1^+ b_1^-$ , and  $b_2 = b_2^+ b_2^-$ . Additionally, the following variables were introduced for a more compact solution representation:

$$b_1^+ = e^{-ikn_m(l+d)} + b_5^-(n_o - n_m)e^{-ikn_o d} - b_5^+(n_m + n_o)e^{ikn_o d},$$

$$b_1^- = b_5^+(n_o - n_m)e^{ikn_o d} - b_5^-(n_m + n_o)e^{-ikn_o d},$$

$$b_2^+ = e^{-ikn_m(l+d)} + b_6^-(n_o - n_m)e^{-ikn_o d} - b_6^+(n_o + n_m)e^{ikn_o d},$$

$$b_2^- = b_6^+(n_o + n_m)e^{-ikn_o d} - b_6^-(n_o - n_m)e^{ikn_o d},$$

$$b_3^\pm = (-1)^{mp} n_s k e^{\pm ik\bar{n}L} \mp b_7^\pm, \quad (10)$$

$$b_4^\pm = (1 \mp n_m) e^{ikn_m l},$$

$$b_5^\pm = kr_m \chi_m (n_o \mp \bar{n}) + k\chi_{-m} (n_o \pm \bar{n}) \pm \eta_m,$$

$$b_6^\pm = r_m (kn_o^\pm \mp \chi_m) + kn_o^\mp \pm \chi_{-m},$$

$$b_7^\pm = e^{\pm i\delta L} (k\bar{n} - \chi_{\mp m}).$$

### III. SPECTRA OF REFLECTANCE, TRANSMITTANCE, AND INTENSITY AMPLIFICATION

To conduct numerical calculations, let us consider the structure, which consists of layers of silver (Ag), NLC, and DBR. The latter is made of repeating layers of TiO<sub>2</sub> and SiO<sub>2</sub>, with refractive indices and thicknesses of  $n_{\text{TiO}_2}$ ,  $d_{\text{TiO}_2}$  and  $n_{\text{SiO}_2}$ ,  $d_{\text{SiO}_2}$ , respectively. The values of the structure parameters used in the calculations are presented in Table I. It should be noted that in Ref. 74, similar Tamm plasmonic modes in the visible spectrum were experimentally detected in a similar layered structure Ag-DBR but without the NLC layer. For the DBR structure, we choose the period of its

of the reflected wave  $B_0$  and the transmitted wave  $A_4$ , from which we obtain the reflection  $R$  and transmission  $T$  coefficients of the structure,

variation,  $a = d_{\text{TiO}_2} + d_{\text{SiO}_2} = 147$  nm. For the chosen thicknesses of the TiO<sub>2</sub> and SiO<sub>2</sub> layers, the DBR's bandgap covers the range of wavelengths of the incident light within 450–650 nm. The thickness of the DBR layer was chosen to be  $L = 1764$  nm, corresponding to  $p = 12$  periods of its structural variation. The value of the complex refractive index  $n_m$  of the Ag layer, taken from Ref. 75 for the calculation, accounts for its frequency dispersion.

The numerically calculated dependencies of the reflection coefficient  $R$ , transmission coefficient  $T$ , and absorption coefficient  $A$  (where  $R + T + A = 1$ ) of the specified system on the wavelength  $\lambda$  of the incident wave are shown in Fig. 2. The calculations of the spectral dependencies of the coefficients  $R$ ,  $T$ , and  $A$  were conducted using the finite element method in COMSOL Multiphysics. The obtained numerical results were verified by applying the transfer matrix method. It should be noted that narrow dips in the reflection spectrum and peaks in the transmission spectrum of the system correspond to the bandgap region of the DBR (Fig. 2, solid blue lines). The presence of these dips/peaks in the reflection/transmission spectra is associated with the excitation of TPPs at the interface of the Ag-NLC layers. The dips in the  $R$  coefficient and peaks in the  $T$  values correspond to peaks in the  $A$  coefficient. As the calculations show, the number of dips/peaks in the spectral dependencies of the reflection/transmission coefficients, as well as absorption, increases with the increase in the thickness of the NLC layer.

In Fig. 2, the values of the reflection coefficient  $R$ , transmission coefficient  $T$ , and absorption coefficient  $A$  calculated according to formulas (9) and (10) are also presented for comparison. The values of  $\epsilon_0$  and  $\epsilon_j$  (where  $j \neq 0$ ) used for the calculation are obtained from the Fourier series decomposition (3) of the dielectric permittivity  $\epsilon(z)$  of the DBR medium,

$$\epsilon_0 = \frac{n_{\text{TiO}_2}^2 d_{\text{TiO}_2} + n_{\text{SiO}_2}^2 d_{\text{SiO}_2}}{d_{\text{TiO}_2} + d_{\text{SiO}_2}}, \quad (11)$$

$$\epsilon_j = i \frac{n_{\text{SiO}_2}^2 - n_{\text{TiO}_2}^2}{2\pi j} (1 - e^{-i2\pi j d_{\text{TiO}_2}/a}), \quad (12)$$

where  $j \neq 0$ . As can be seen from Fig. 2, there is a good agreement between the results of the numerical calculation and the analytical expressions (9), represented by solid black and dotted red lines, respectively.

The numerically calculated spectral dependence of the localization coefficient  $\gamma = |E|^2/|A_0|^2$  of the light wave intensity in the

TABLE I. Parameter values used for calculations.

Parameter	Value	Description
$l$	60 nm	Ag layer thickness
$d$	3287 nm	NLC layer thickness
$d_{\text{TiO}_2}$	51 nm	TiO <sub>2</sub> layer thickness
$d_{\text{SiO}_2}$	96 nm	SiO <sub>2</sub> layer thickness
$n_o$	1.48	NLC ordinary refractive index
$n_e$	1.63	NLC extraordinary refractive index
$n_{\text{TiO}_2}$	2.46	TiO <sub>2</sub> refractive index
$n_{\text{SiO}_2}$	1.48	SiO <sub>2</sub> refractive index
$n_s$	1.529	Substrate refractive index

05 June 2024 19:19:54

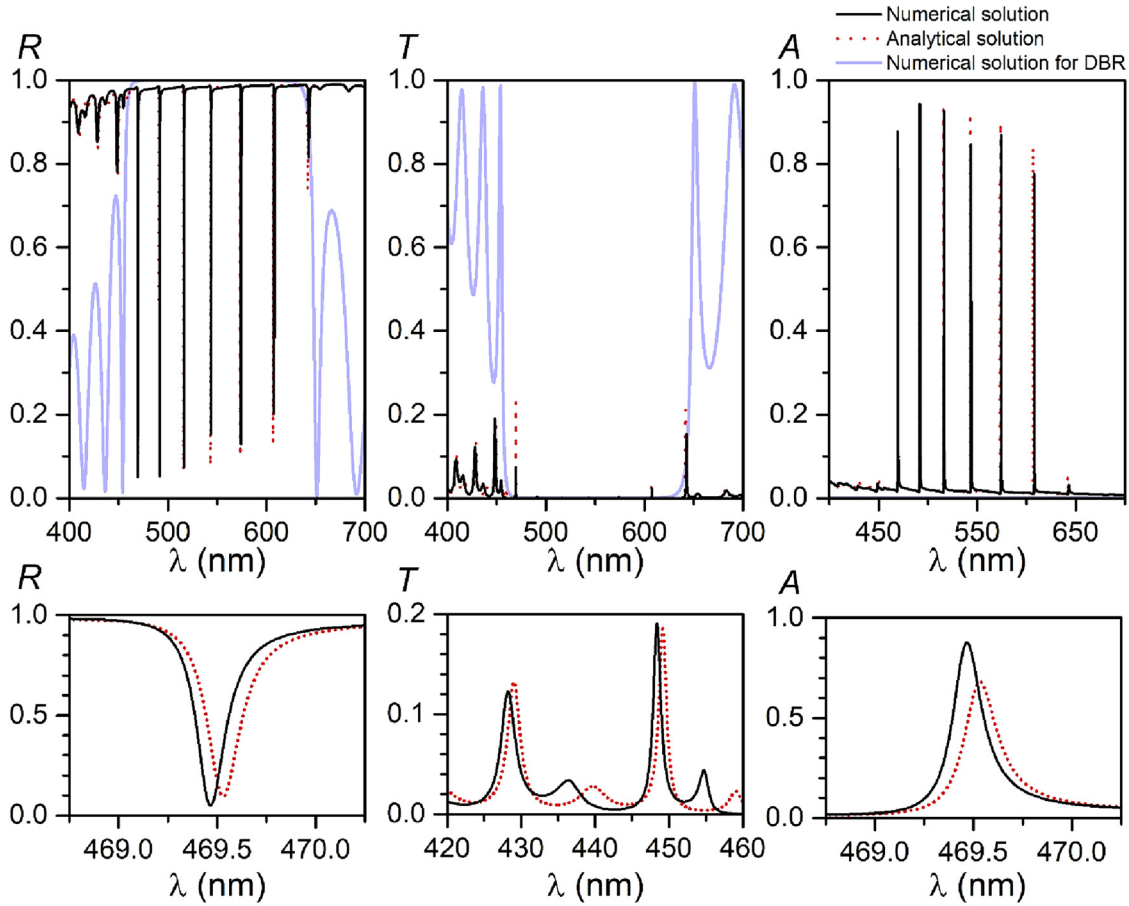


**FIG. 2.** Top row: spectral dependencies of the reflectance ( $R$ ), transmittance ( $T$ ), and absorbance ( $A$ ), according to the numerical solution (solid black lines) and the analytical solution (dotted red lines). Bottom row: Enlarged views of the reflectance, transmittance, and absorbance peaks. Reflectance and absorbance peaks are localized within the DBR bandgap (solid blue lines).

05 June 2024 19:19:54

NLC layer is shown in Fig. 3(a). The  $\gamma$  coefficient is defined as the ratio of the volume-averaged intensity  $|E|^2$  within NLC to the intensity  $I_0 = |A_0|^2$  of the incident light. Thus, at wavelengths  $\lambda$  corresponding to the peaks of the gain coefficient  $\gamma$  (dips in the reflection coefficient spectrum), excitation of Tamm plasmons occurs. As can be seen, this is accompanied by a significant increase in the intensity of the light wave inside the volume of NLC compared to the intensity of the incident light. Under the parameters assumed for the calculation, the localization coefficient  $\gamma$  almost reaches the value of 60.

Figure 3(b) shows the distribution of the dimensionless intensity  $\tilde{I}(z) = |E|^2/|A_0|^2$  of the light wave across the thickness of the system, numerically obtained at a wavelength  $\lambda$  close to the Bragg wavelength  $\lambda_B = 552$  nm. As can be seen, the light wave field is almost entirely localized within the NLC layer and is uniformly distributed across its thickness with spatially modulated intensity. In the NLC medium, the values of the local intensity maxima are

found to be twice as large as the volume-averaged intensity in NLC. Compared to the intensity  $I_0$  of the incident light, the values of the local maxima of the light intensity in the NLC layer are found to be about 110 times larger. As the light wave enters the DBR structure, it quickly attenuates so that the light field is practically absent within the dielectric substrate that follows the DBR. This corresponds to the case of no light transmission through the system,  $T = 0$ .

The values of the wavelengths  $\lambda$  of the incident light at which the excitation of Tamm plasmons occurs depend significantly on the optical parameters (dielectric constants) of the NLC layer. The values of these parameters depend directly on the ordering state within the volume of NLC, namely, on the director's orientation. For example, in the case of a homogeneous planar orientation of the NLC layer, in equations (1) for the electric field intensity vectors  $\vec{E}_i$  and magnetic field intensity vectors  $\vec{H}_i$ , the refractive index value  $n_{LC}$  needs to be changed from  $n_o$  to  $n_e$ , where  $n_e$  is the refractive index of the extraordinary ray in NLC.

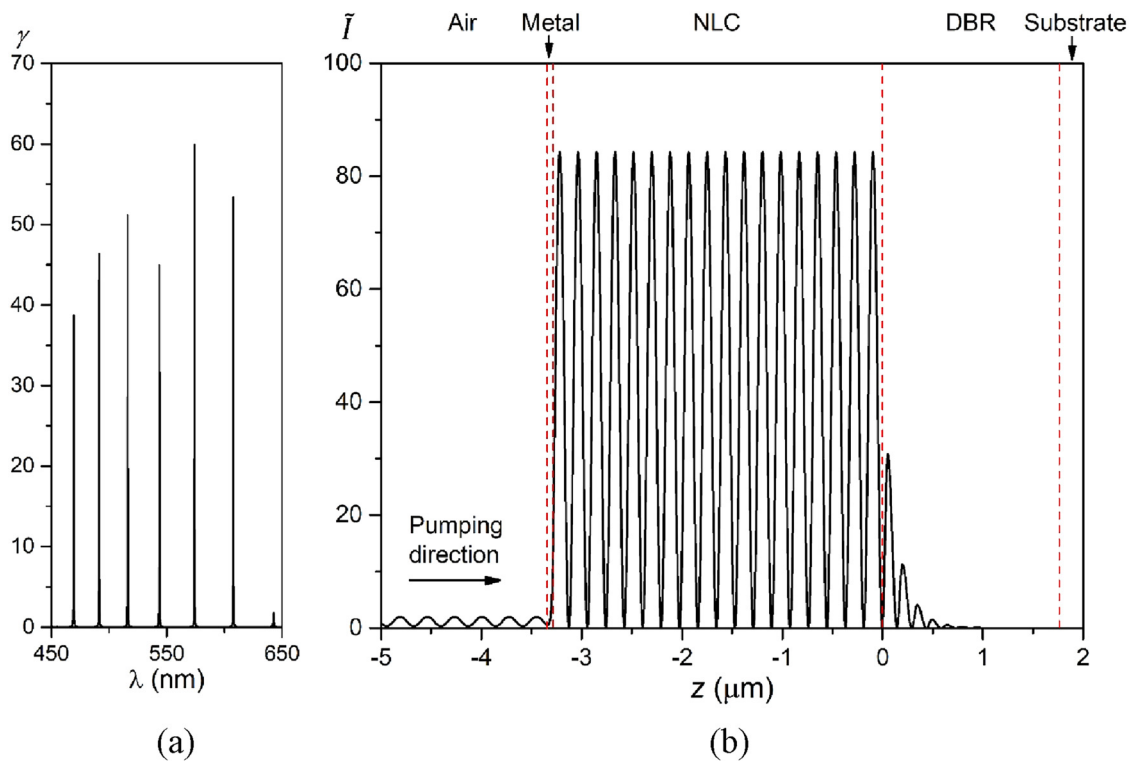


**FIG. 3.** (a) Spectral dependence of the localization coefficient  $\gamma$  of the light field intensity in the NLC layer. (b) Distribution of the dimensionless intensity  $\tilde{I}$  obtained at the wavelength  $\lambda = 543.7$  nm.

Figures 4(a) and 4(b) demonstrate the changes in the spectra of reflection and light intensity localization coefficient, resulting from a change in the orientation from homeotropic to planar. Two NLC layer materials with the extraordinary indexes of 1.63 (red lines) and 1.78 (blue lines), corresponding to the optical anisotropies  $\Delta n = n_e - n_o$  of 0.15 and 0.3, respectively, are presented. The NLC reorientation induces a shift of plasmonic peaks toward longer wavelengths. This shift is sensitive to changes in the refractive index values of the NLC medium and, consequently, the magnitude of its optical anisotropy. For the case of an optical anisotropy in NLC of  $\Delta n = 0.15$ , the shift of plasmonic peaks reaches 50 nm [red arrow in Fig. 4(a)], and for a high-anisotropy NLC with  $\Delta n = 0.3$ ,<sup>76</sup> the corresponding shift reaches 100 nm [blue arrow in Fig. 4(a)]. It should be noted that the spectral distribution of peak amplitudes qualitatively remains practically unchanged. The consideration of two extreme cases of NLC layer orientation, homeotropic and planar, allows us to estimate the nature and range of the influence of the NLC layer's orientation on the characteristics of Tamm plasmon excitation.

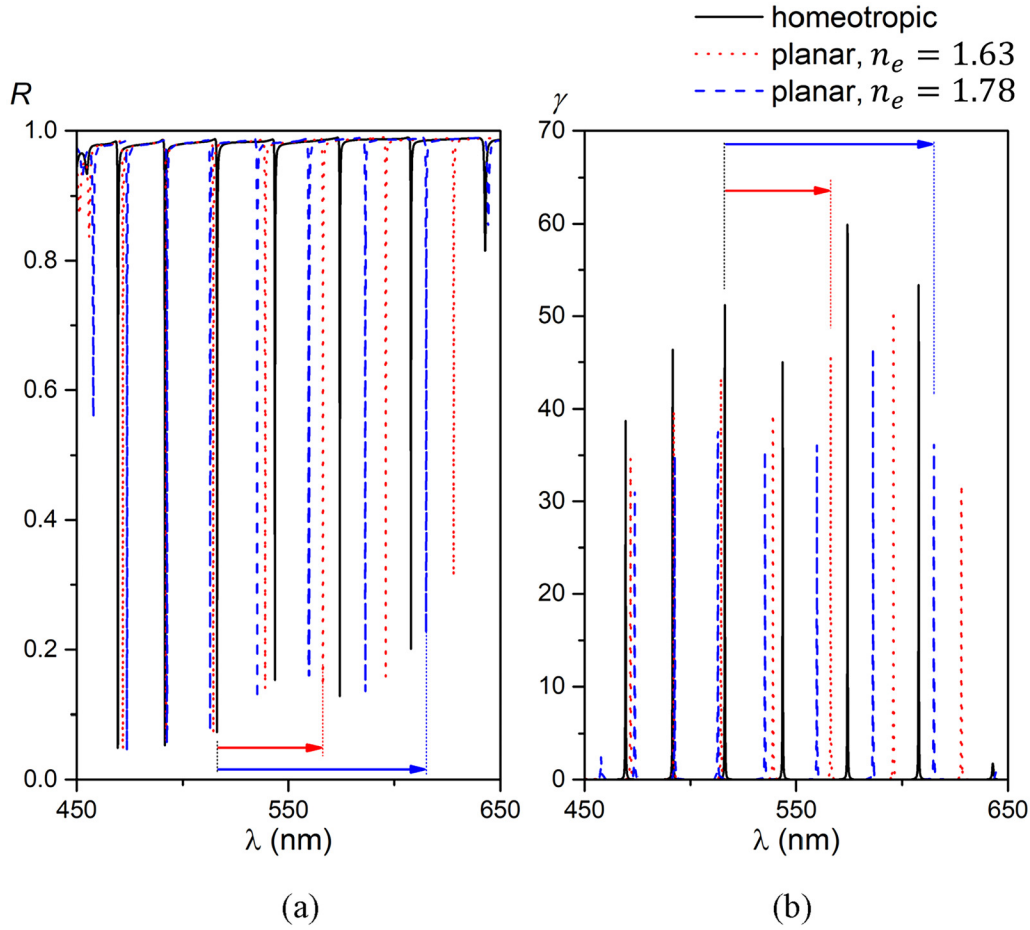
Changes in the spectrum of the gain coefficient  $\gamma$  of the light wave and the distribution of its intensity  $\tilde{I}$  throughout the thickness of the system are caused by the addition of a small concentration of light-absorbing dye into the NLC. This is illustrated in Fig. 5. For simplicity in the calculation, we assume that the

absorption of incident light by the dye is uniformly distributed across the wavelengths  $\lambda$ . The presence of light-absorbing dye in the volume of NLC results in the appearance of an imaginary part in the refractive index of the NLC medium. Numerically calculated dependencies of the gain coefficient  $\gamma$  of the light wave in the NLC layer on the wavelength  $\lambda$  of the incident light are shown in Fig. 5(a). The presence of the dye leads to a significant reduction in the value of the localization coefficient  $\gamma$  of the light wave intensity. However, the positions of the plasmonic peaks remain practically unchanged. The relative spectral distribution of the plasmonic peaks also remains almost unchanged. The distribution of the dimensionless intensity  $\tilde{I}$  of the light wave along the  $z$  coordinate is shown in Fig. 5(b). Similar to the localization coefficient  $\gamma$ , the distribution of the intensity  $\tilde{I}$  of the light wave remains homogeneous, spatially modulated, and overall qualitatively unchanged, except for the amplitude reduction due to absorption.

#### IV. MODELING OF LASER GENERATION

In this section, we consider the features of laser generation in the hybrid structure Ag-NLC-DBR. Studying laser generation in such a structure requires an understanding of the system's behavior in the presence of population inversion in the amplifying





05 June 2024 19:19:54

**FIG. 4.** Spectral dependencies of the values of the reflection coefficients  $R$  (a) and the amplification  $\gamma$  (b) of the intensity of the light field in the NLC layer. The cases of homeotropic ( $n_o = 1.48$ , solid black line) and planar ( $n_e = 1.63$ , dotted red line;  $n_e = 1.78$ , dashed blue line) NLC orientations are presented. The arrows indicate how a reference plasmonic peak is shifted due to LC reorientation.

medium. In the considered structure, the role of the amplifying medium is played by the NLC medium doped with a light-absorbing dye. The presence of population inversion in the levels of the NLC medium leads to the appearance of a negative imaginary part in the refractive index of the dye. As a result, this generally leads to the presence of a negative imaginary part in the refractive index of the dye-doped NLC medium as a whole. It is assumed that the magnitude of the imaginary part of the refractive index of the dye-doped NLC medium is directly proportional to the concentration of the dye and does not depend on the wavelength  $\lambda$  of the incident light.

The lasing generation is modeled within the framework of singlet and triplet energy levels of the dye such as 4-dicyanomethylene-2-methyl-6-dimethylaminostryryl-4H-pyran (DCM) (see Fig. 6). This model requires solving three (four counting the equation for  $N$ ) rate equations describing the population densities in the ground singlet  $N_1$ , excited singlet  $N_2$ , and

ground triplet  $N_3$  energy states and generated light emission intensity  $I_e$ ,<sup>31,68,77</sup>

$$\begin{aligned} \frac{\partial N_2(z, t)}{\partial t} &= \frac{\sigma_a I_a(z, t)}{h\nu_a} N_1(z, t) - \frac{\sigma_e I_e(t)}{h\nu_e} N_2(z, t) - \frac{N_2(z, t)}{\tau_{21}} - P_{23} N_2(z, t), \\ \frac{\partial N_3(z, t)}{\partial t} &= P_{23} N_2(z, t) - P_{31} N_3(z, t), \\ \frac{dI_e(t)}{dt} &= \frac{ch\nu_e S}{\bar{n}V} \int_0^L \left( \frac{\sigma_e I_e(t)}{h\nu_e} N_2(z, t) + k \frac{N_2(z, t)}{\tau_r} \right) dz - \frac{I_e(t)}{\tau_c}, \\ N_1(z, t) + N_2(z, t) + N_3(z, t) &= N, \end{aligned} \quad (13)$$

where the transition probabilities are taken in the form of

$$W_{12} = \frac{\sigma_a I_a}{h\nu_a}, \quad W_{21} = \frac{\sigma_e I_e}{h\nu_e}, \quad W_{sp} = \frac{1}{\tau_{21}}. \quad (14)$$

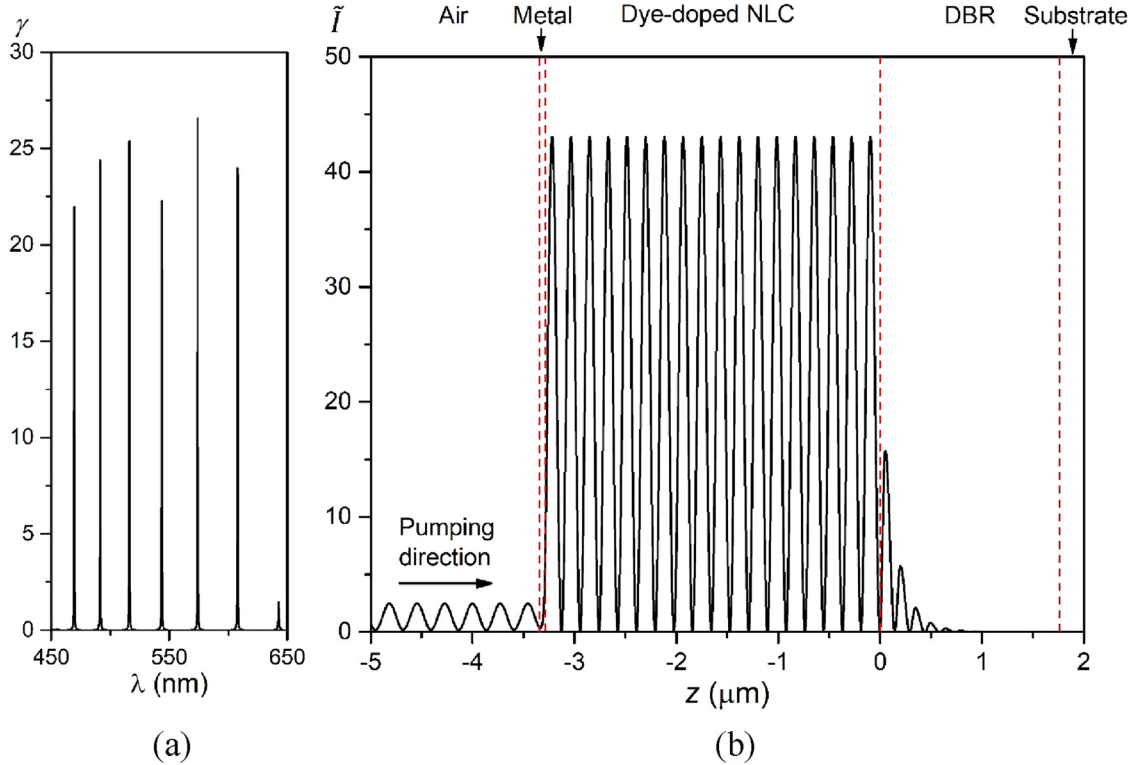


FIG. 5. Spectral dependency of the localization coefficient  $\gamma$  (a) of the light field intensity and the distribution of the dimensionless intensity  $\tilde{I}$  (b) of the light wave across the thickness of the structure in the presence of absorption in the NLC layer at  $\lambda = 543.7$  nm,  $n_o = 1.48 + 0.0001i$ .

05 June 2024 19:19:54

In the expressions (13) and (14),  $N_i$  is the population of the corresponding energy levels;  $W_{ij}$  and  $P_{ij}$  are the probabilities of induced and intercombination transitions from level  $i$  to level  $j$  (where  $i, j = 1, 2, 3$ );  $W_{sp}$  and  $\tau_{21}$  represent the probability and

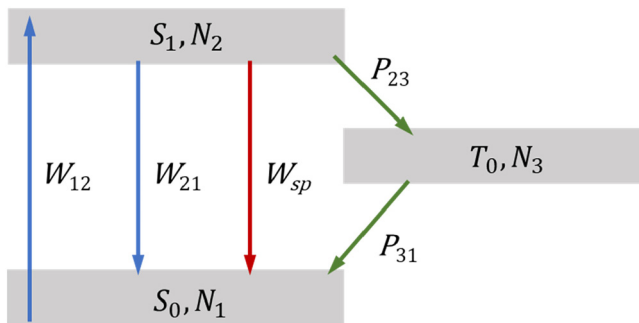


FIG. 6. Diagram of the energy levels representing the dye-doped system.  $W_{12}$  and  $W_{21}$  denote the probabilities of induced transitions between the singlet levels  $S_1$  and  $S_2$ ;  $W_{sp}$  stands for the probability of the spontaneous transition from  $S_2$  to  $S_1$ ;  $P_{23}$  and  $P_{31}$  denote the probabilities of intercombination transitions.

characteristic lifetime of fluorescence;  $\tau_r$  is the lifetime of radiative spontaneous emission;  $I_a$  and  $I_e$  are the intensities of absorbed and emitted light, respectively;  $\tau_c$  is the characteristic lifetime of the laser mode in the cavity; and  $k$  denotes the fraction of radiation propagating along the laser's main axis.

Solving the system of equations (13) for the population of energy levels requires averaging all quantities within the active medium. For the previously obtained values of the localization coefficient  $\gamma$  of the light wave intensity in the NLC medium, the spatial distribution of the pump intensity can be approximated reasonably well as  $I_a = I_{a0} \sin^2 qx$  (see Fig. 5). As a result, the system of equations for the population of levels (13) becomes significantly simplified,

$$\begin{aligned} \frac{dn_2}{dt} &= -\left(\frac{\sigma_e P_e}{h\nu_e S} + \frac{1}{\tau_{21}} + P_{23} + \frac{3\sigma_a P_{a0}}{4h\nu_a S}\right)n_2 - \frac{3\sigma_a P_{a0}}{4h\nu_a S}n_3 + \frac{\sigma_a N P_{a0}}{2h\nu_a S}, \\ \frac{dn_3}{dt} &= P_{23}n_2 - P_{31}n_3, \\ \frac{dP_e}{dt} &= \frac{c}{n} \left(\sigma_e P_e + k \frac{h\nu_e S}{\tau_r}\right)n_2 - \frac{P_e}{\tau_c}, \end{aligned} \quad (15)$$

where  $P_e = I_e S$  and  $P_{a0} = I_{a0} S$  stand for the radiation and absorption powers, respectively, and  $n_i$  denotes the mean level population

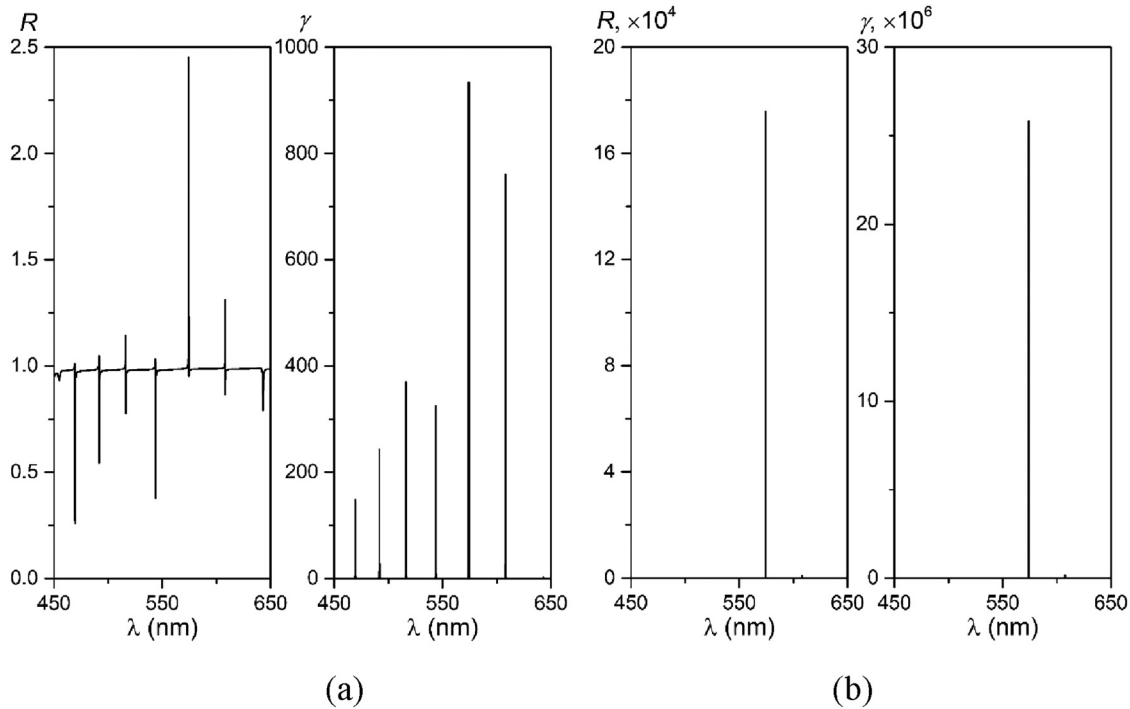


FIG. 7. Spectral dependencies of the reflection coefficient  $R$  and the intensity amplification  $\gamma$ . (a)  $n_o = 1.48 - 0.00015i$ ; (b)  $n_o = 1.48 - 0.0002i$ .

across the dye-doped NLC layer,

$$n_i = \frac{1}{L} \int_0^L N_i(z, t) dz, \quad i = 1, 2, 3.$$

The results of numerical calculations for the spectral dependencies of the reflection coefficient  $R$  and the localization coefficient  $\gamma$  of the light wave are presented in Fig. 7. The presence of a relatively small gain in the system due to the negative imaginary part of the refractive index of the dye-doped NLC,  $n_o = 1.48 - 0.00015i$ , results in the reflection coefficient  $R$  of the system becoming larger than unity at the excitation frequencies of TPPs [see Fig. 7(a)]. This leads to a significant increase in the value of the localization coefficient  $\gamma$  of the light field intensity within the dye-doped NLC medium, reaching 900 units of the incident wave intensity. Consequently, the intensity of the light field within the dye-doped NLC medium increases to the extent that the intensity of the reflected light wave leaving the system through the metal layer (reflected light wave) becomes larger than the intensity of the incident (seed) light wave. This corresponds to the phenomenon of laser generation in the system under consideration.

Furthermore, a relatively small increase in the absolute value of the negative imaginary part of the refractive index of dye-doped NLC to  $\text{Im}(n_o) = -0.0002$ , resulting in  $n_o = 1.48 - 0.0002i$ , leads to a rapid increase in the value of the system's reflection coefficient

$R$ , by more than two orders of magnitude [see Fig. 7(b)]. In this case, the value of the localization coefficient  $\gamma$  of the light field intensity within the dye-doped NLC medium also increases and reaches magnitudes of  $10^7$ . With such values of the gain coefficient  $\gamma$ , laser generation in the system can start spontaneously, as fluctuations in the intensity of the light wave within the NLC medium can act as the seed waves.

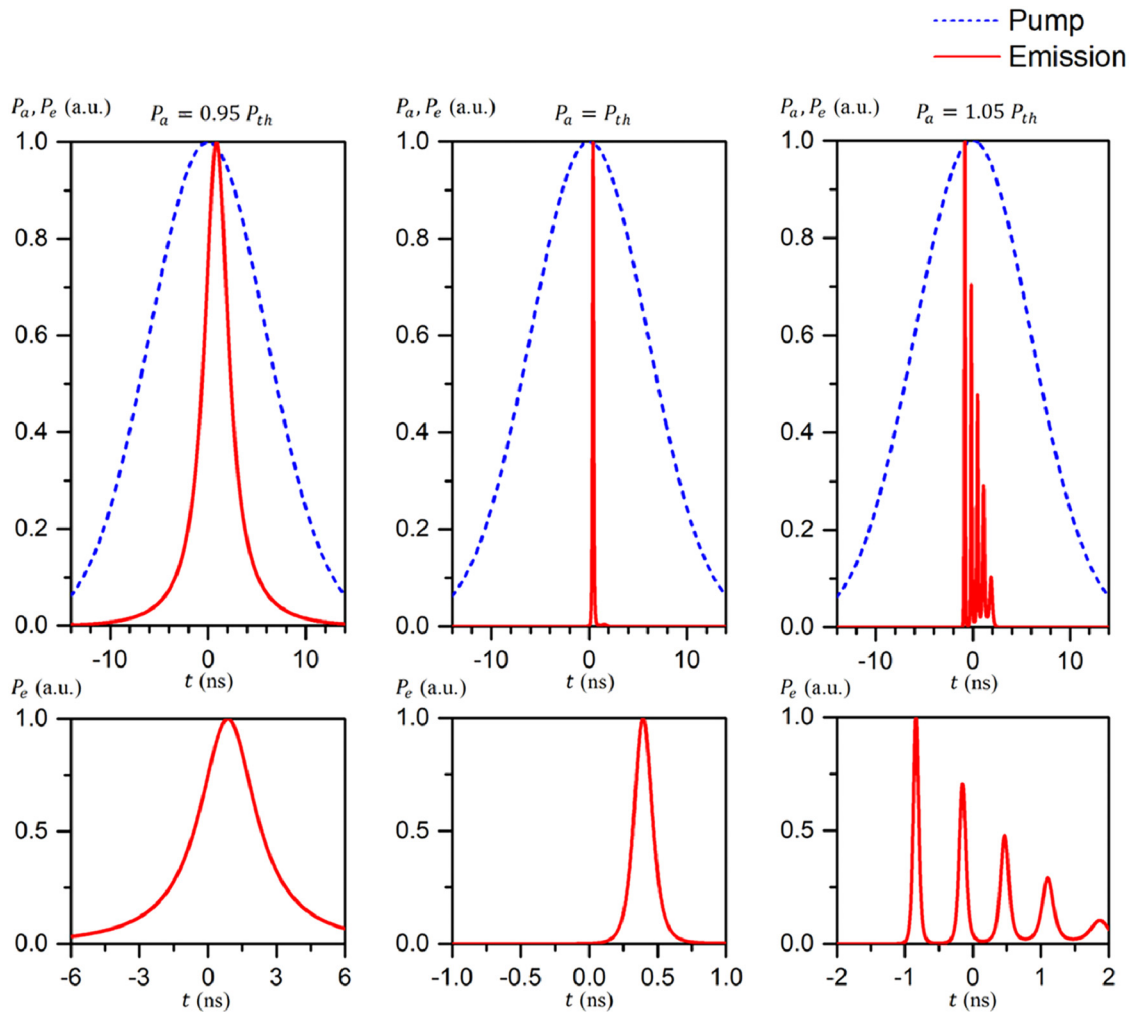
It should be noted that the increase in the value of the reflection coefficient  $R$ , caused by the increase in the absolute value of the negative imaginary part of the refractive index of dye-doped NLC, is accompanied by a redistribution of amplitudes between the Tamm plasmon peaks in the spectra of reflection coefficients  $R$  and gain coefficients  $\gamma$  of the light field. For instance, in the case of the refractive index of dye-doped NLC being  $n_o = 1.48 - 0.0002i$ , almost all of the intensity of the light wave within the dye-doped NLC medium is concentrated within a single peak at a wavelength of  $\lambda = 574$  nm, while other plasmonic peaks have amplitudes that are two orders of magnitude smaller [see Fig. 7(b)].

Next, we simulate the process of laser generation in the system under consideration by directly solving the system of equations (15) for the population of energy levels. The calculation was performed for typical parameter values,<sup>31,68,77</sup> as summarized in Table II. Figure 8 shows the normalized temporal profiles of the laser generation pulses for different pump pulse power settings relative to the lasing threshold power. It should be noted that the laser generation threshold in the considered system, for the parameter values taken

05 June 2024 19:19:54

TABLE II. Values of the parameters used in the equations for the population densities of energy levels.<sup>31,68,77</sup>

Parameter	Value	Reference	Description
$P_{31}$	$10^4 \text{ s}^{-1}$	77	Probability of transition from triplet level
$P_{23}$	$5 \times 10^7 \text{ s}^{-1}$	77	Probability of transition to triplet level
$\tau_{21}$	$1.2 \times 10^{-9} \text{ s}$	68	Fluorescence lifetime
$\tau_a$	$14 \times 10^{-9} \text{ s}$	...	Temporal width of the pumping pulse
$\tau_c$	$5.38 \times 10^{-13} \text{ s}$	...	Radiation lifetime
$\tau_r$	$2.4 \times 10^{-9} \text{ s}$	68	Lifetime of radiative spontaneous emission
$N$	$5.96 \times 10^{24} \text{ m}^{-3}$	...	Dye concentration in the NLC
$\beta$	$10^4 \text{ m}^{-1}$	68	Coefficient of distributed losses
$\sigma_e$	$1.53 \times 10^{-20} \text{ m}^2$	31	Cross section of induced emission
$\sigma_a$	$0.62 \times 10^{-20} \text{ m}^2$	31	Cross section of absorption
$S$	$8.01 \times 10^{-10} \text{ m}^2$	...	Cross-sectional area of pumping region
$\lambda_a$	445 nm	77	Pumping wavelength
$\lambda_e$	600 nm	77	Emission wavelength



05 June 2024 19:19:54

FIG. 8. Top row: temporal profiles of normalized pumping and laser emission pulses below, at, and above the lasing threshold, respectively. Bottom row: enlarged views of the laser emission pulses.

above, is observed at a pump pulse power of  $P_{th} = 7.4$  W, which corresponds to the pumping intensity of  $9.2$  MW/cm<sup>2</sup>.

At the laser generation threshold, luminescence is accompanied by a single pulse. With increasing supra-threshold pump power values, luminescence manifests as a series of short generation pulses with a monotonically decreasing amplitude. The latter can be explained by the fact that after reaching the threshold population of dye molecules on the excited singlet level, depletion of this level to the triplet states occurs, leading to the cessation of generation. Unlike the case of pump power values below the laser generation threshold, in the supra-threshold regime, the first most intense luminescence pulse leads ahead of the maximum of the pump pulse. With an increase in pump power, the duration of luminescence pulses decreases below the laser generation threshold. Moreover, this trend persists for pump power values above the laser generation threshold when considering the first luminescence peaks. It is worth noting that, overall, the temporal profiles of generation in the considered hybrid structure Ag-NLC-DBR are qualitatively similar to those obtained in previous works<sup>31,68,77</sup> in the case of the CLC laser with distributed feedback.

## V. DISCUSSION AND CONCLUSIONS

In this work, controlled laser generation in the Ag-NLC-DBR hybrid structure using NLC has been theoretically investigated. Within the scope of our research, numerical calculations have been performed for the spectral dependencies of the coefficients of reflection, transmission, and absorption of light by such a system. The obtained narrow dips in the reflection coefficient and peaks in the transmission and absorption coefficients are attributed to the excitation of TPPs at the Ag-NLC boundary. It has been established that increasing the thickness of the NLC layer leads to an increase in the density of Tamm plasmon peaks. The excitation of TPPs is accompanied by a significant increase (approximately 55 times) in the intensity of the light field within the NLC medium compared to the intensity of the incident light. Moreover, the light field is almost entirely localized within the NLC layer with spatially modulated intensity. We have proposed an analytical approach to describe the problem when the wavelength of the incident light is close to the Bragg wavelength. It should be noted that such an approach adequately describes the positions and magnitudes of TPP peaks even when the mentioned condition is slightly violated.

The influence of the orientation of the NLC layer on the positions and magnitudes of the TPP excitation dips/peaks has been studied. It has been shown that changing the orientation of the NLC layer from homeotropic to planar leads to an increase in the refractive index of the incident light within the NLC medium and, consequently, to a shift of plasmon peaks toward longer wavelengths. As a result, the use of NLC ( $n_o = 1.48$ ,  $n_e = 1.78$ ) allows for a shift of plasmon peaks within the 100 nm range. It should be noted that achieving a shift of plasmon peaks within the substantial range of 100 nm is not feasible for NLC in the absence of Tamm plasmons. Clearly, the orientation of the NLC layer affects the wavelength of TPP excitation, which, in turn, influences the properties and characteristics of laser generation in the studied system. By applying external stimuli such as electric fields, magnetic fields, or heat, one can change the LC director orientation and the order

parameter. This leads to corresponding changes in the components of the dielectric tensor, thereby allowing the tuning or control of lasing. Detailed calculations (for instance, the LC director reorientation under a given applied voltage, and the lasing threshold vs voltage) are beyond the scope of the current study.

The addition of a small concentration of light-absorbing dye molecules to the NLC volume does not change the positions and relative spectral distribution of the plasmon peaks. The presence of the dye leads to a decrease in the amplification of light intensity in the dye-doped NLC medium without altering the nature of the intensity distribution throughout its thickness. At the same time, it should be noted that the presented model assumes a perfect broadband fluorescent emitter over the tuning range. In practice, gain would be limited to the fluorescence band of the chosen emitter. However, some organic laser dyes have wide fluorescence bands that would feasibly still allow a 100 nm tuning range.

The peculiarities of laser generation in the Ag-NLC-DBR system were investigated under conditions of inverted population levels in the dye-doped NLC medium doped with a light-absorbing dye. The presence of a relatively small negative imaginary part of the refractive index in the dye-doped NLC,  $-0.0002$ , resulting from inverted level populations, leads to an increase in the reflection coefficient by more than two orders of magnitude. Meanwhile, the localization coefficient of the light intensity in the dye-doped NLC medium reaches the order of  $10^7$ . It should be noted that adding an azo-dye with light-induced *trans-cis* isomerization to NLC will lead to a change in the order parameter of the system. As a result, both the ordinary and extraordinary refractive indices of NLC change. Thus, by changing the orientation of the NLC using an external electric or magnetic field, it is possible to influence the value of the lasing wavelength.

By directly solving the system of equations for the level population, we obtained the time dependencies of the emission pulses for the pump powers below, at, and above the laser generation threshold. As the calculations show, an increase in the pump power leads to a reduction in the duration of luminescence pulses. For pump power values above the laser generation threshold, luminescence in the system manifests as a series of short pulses, with the amplitude exhibiting a monotonic decrease over time.

In conclusion, the proposed Tamm-plasmon hybrid structure Ag-NLC-DBR is a convenient system for laser generation due to its high level of intensity amplification and the ability to control this amplification in real-time using NLC. This can have significant implications in applied fields of optoelectronics and photonics where precise manipulation of laser emission is of great importance.

## ACKNOWLEDGMENTS

This research was funded by the University of Edinburgh—Taras Shevchenko National University of Kyiv Partnership Fund and the UK Engineering and Physical Sciences Research Council (EPSRC) studentship for I.P. (Grant No. EP/T517884/1).

## AUTHOR DECLARATIONS

### Conflict of Interest

The authors have no conflicts to disclose.

## Author Contributions

**I. I. Yakovkin:** Data curation (equal); Formal analysis (equal); Investigation (lead); Methodology (equal); Software (equal); Validation (equal); Visualization (equal); Writing – original draft (equal); Writing – review & editing (equal). **M. F. Ledney:** Data curation (equal); Formal analysis (equal); Funding acquisition (supporting); Investigation (equal); Methodology (equal); Resources (equal); Software (equal); Supervision (equal); Validation (equal); Visualization (equal); Writing – original draft (equal); Writing – review & editing (equal). **V. Yu. Reshetnyak:** Conceptualization (equal); Formal analysis (equal); Funding acquisition (supporting); Investigation (supporting); Methodology (supporting); Resources (equal); Software (supporting); Writing – review & editing (equal). **I. Pakamoryte:** Data curation (equal); Formal analysis (equal); Investigation (equal); Methodology (equal); Resources (equal); Software (equal); Validation (equal); Writing – review & editing (equal). **P. J. W. Hands:** Conceptualization (equal); Formal analysis (equal); Funding acquisition (lead); Investigation (supporting); Methodology (supporting); Project administration (equal); Resources (equal); Supervision (equal); Writing – review & editing (equal).

## DATA AVAILABILITY

The data that support the findings of this study are available from the corresponding author upon reasonable request.

## REFERENCES

- 1 J. A. Gaspar-Armenta and F. Villa, *J. Opt. Soc. Am. B* **20**, 2349 (2003).
- 2 A. V. Kavokin, I. A. Shelykh, and G. Malpuech, *Phys. Rev. B* **72**, 233102 (2005).
- 3 A. P. Vinogradov, A. V. Dorofeenko, S. G. Erokhin, M. Inoue, A. A. Lisyansky, A. M. Merzlikin, and A. B. Granovsky, *Phys. Rev. B* **74**, 045128 (2006).
- 4 M. Kaliteevski, I. Iorsh, S. Brand, R. A. Abram, J. M. Chamberlain, A. V. Kavokin, and I. A. Shelykh, *Phys. Rev. B* **76**, 165415 (2007).
- 5 M. E. Sasin, R. P. Seisyan, M. A. Kaliteevski, S. Brand, R. A. Abram, J. M. Chamberlain, A. Y. Egorov, A. P. Vasil'ev, V. S. Mikhlin, and A. V. Kavokin, *Appl. Phys. Lett.* **92**, 251112 (2008).
- 6 M. E. Sasin, R. P. Seisyan, M. A. Kaliteevski, S. Brand, R. A. Abram, J. M. Chamberlain, I. V. Iorsh, I. A. Shelykh, A. Y. Egorov, A. P. Vasil'ev, V. S. Mikhlin, and A. V. Kavokin, *Superlatt. Microstruct.* **47**, 44 (2010).
- 7 T. Goto, A. V. Dorofeenko, A. M. Merzlikin, A. V. Baryshev, A. P. Vinogradov, M. Inoue, A. A. Lisyansky, and A. B. Granovsky, *Phys. Rev. Lett.* **101**, 113902 (2008).
- 8 A. M. Vyunishev, R. G. Bikbaev, S. E. Svyakhovskiy, I. V. Timofeev, P. S. Pankin, S. A. Evlashin, S. Y. Vetrov, S. A. Myslivets, and V. G. Arkhipkin, *J. Opt. Soc. Am. B* **36**, 2299 (2019).
- 9 K. R. Welford, J. R. Sambles, and M. G. Clark, *Liq. Cryst.* **2**, 91 (1987).
- 10 M. E. Caldwell and E. M. Yeatman, *Appl. Opt.* **31**, 3880 (1992).
- 11 Y. Wang, *Appl. Phys. Lett.* **67**, 2759 (1995).
- 12 Y. Wang, S. D. Russell, and R. L. Shimabukuro, *J. Appl. Phys.* **97**, 023708 (2004).
- 13 W. Dickson, G. A. Wurtz, P. R. Evans, R. J. Pollard, and A. V. Zayats, *Nano Lett.* **8**, 281 (2008).
- 14 K. R. Daly, S. Abbott, G. D'Alessandro, D. C. Smith, and M. Kaczmarek, *J. Opt. Soc. Am. B* **28**, 1874 (2011).
- 15 S. B. Abbott, K. R. Daly, G. D'Alessandro, M. Kaczmarek, and D. C. Smith, *Opt. Lett.* **37**, 2436 (2012).
- 16 S. B. Abbott, Ph.D. dissertation, University of Southampton, 2012.
- 17 A. I. Lesiuk, M. F. Ledney, and V. Y. Reshetnyak, *Phys. Rev. E* **106**, 024706 (2022).
- 18 V. Y. Reshetnyak, V. I. Zadorozhnyi, I. P. Pinkevych, and D. R. Evans, *Phys. Rev. E* **96**, 022703 (2017).
- 19 I. V. Timofeev, P. S. Pankin, S. Y. Vetrov, V. G. Arkhipkin, W. Lee, and V. Y. Zyryanov, *Crystals* **7**, 113 (2017).
- 20 V. Y. Reshetnyak, V. I. Zadorozhnyi, I. P. Pinkevych, T. J. Bunning, and D. R. Evans, *AIP Adv.* **8**, 045024 (2018).
- 21 P. S. Pankin, V. S. Sutormin, V. A. Gunyakov, F. V. Zelenov, I. A. Tambasov, A. N. Masyugin, M. N. Volochaev, F. A. Baron, K. P. Chen, V. Y. Zyryanov, and S. Y. Vetrov, *Appl. Phys. Lett.* **119**, 161107 (2021).
- 22 V. Y. Reshetnyak, T. J. Bunning, and D. R. Evans, *Liq. Cryst.* **45**, 2010 (2018).
- 23 V. Y. Reshetnyak, V. I. Zadorozhnyi, I. P. Pinkevych, T. J. Bunning, and D. R. Evans, *Materials* **13**, 1523 (2020).
- 24 M. Adams, B. Cemlyn, I. Henning, M. Parker, E. Harbord, and R. Oulton, *J. Opt. Soc. Am. B* **36**, 125 (2019).
- 25 O. Buchnev, A. Belosludtsev, V. Reshetnyak, D. R. Evans, and V. A. Fedotov, *Nanophotonics* **9**, 897 (2020).
- 26 C. Kar, S. Jena, D. V. Udupa, and K. D. Rao, *Opt. Laser Technol.* **159**, 108928 (2023).
- 27 J. Mysliwiec, A. Szukalska, A. Szukalski, and L. Sznitko, *Nanophotonics* **10**, 2309 (2021).
- 28 S. Y. Vetrov, M. V. Pyatnov, and I. V. Timofeev, *J. Opt.* **18**, 015103 (2016).
- 29 M. V. Pyatnov, S. Y. Vetrov, and I. V. Timofeev, *Liq. Cryst.* **44**, 674 (2017).
- 30 V. Y. Reshetnyak, I. P. Pinkevych, T. J. Bunning, M. E. McConney, and D. R. Evans, *Phys. Rev. E* **107**, 014702 (2023).
- 31 J. Ortega, C. Folcia, and J. Etxebarria, *Materials* **11**, 5 (2018).
- 32 A. Chanishvili, G. Chilaya, G. Petriashvili, R. Barberi, M. P. De Santo, M. A. Matranga, and F. Ciuchi, *Appl. Phys. Lett.* **88**, 101105 (2006).
- 33 K. Kaminska, T. Brown, G. Beydaghyan, and K. Robbie, *Appl. Opt.* **42**, 4212 (2003).
- 34 S. Keshavarzi, A. Kovacs, M. Abdo, V. Badilita, R. Zhu, J. G. Korvink, and U. Mescheder, *ECS J. Solid State Sci. Technol.* **8**, Q43 (2019).
- 35 S. Ilyas, T. Böcking, K. Kilian, P. J. Reece, J. Gooding, K. Gaus, and M. Gal, *Opt. Mater.* **29**, 619 (2007).
- 36 P. G. Verly, *Appl. Opt.* **47**, C172 (2008).
- 37 V. Reshetnyak, I. Pinkevych, T. Bunning, and D. Evans, *Materials* **14**, 1282 (2021).
- 38 W. L. Zhang, F. Wang, Y. J. Rao, and Y. Jiang, *Opt. Express* **22**, 14524 (2014).
- 39 B. Auguié, M. C. Fuertes, P. C. Angelomé, N. L. Abdala, G. J. A. A. Soler Illia, and A. Fainstein, *ACS Photonics* **1**, 775 (2014).
- 40 A. V. Baryshev and A. M. Merzlikin, *Appl. Opt.* **53**, 3142 (2014).
- 41 S. Kumar, P. S. Maji, and R. Das, *Sens. Actuators, A* **260**, 10 (2017).
- 42 P. S. Maji, M. K. Shukla, and R. Das, *Sens. Actuators, B* **255**, 729 (2018).
- 43 W. L. Zhang and S. F. Yu, *Opt. Commun.* **283**, 2622 (2010).
- 44 H.-C. Cheng, C.-Y. Kuo, Y.-J. Hung, K.-P. Chen, and S.-C. Jeng, *Phys. Rev. Appl.* **9**, 064034 (2018).
- 45 Y. Gong, X. Liu, H. Lu, L. Wang, and G. Wang, *Opt. Express* **19**, 18393 (2011).
- 46 Z. Yang, S. Ishii, T. Yokoyama, T. D. Dao, M. Sun, T. Nagao, and K. Chen, *Opt. Lett.* **41**, 4453 (2016).
- 47 Z.-Y. Yang, S. Ishii, T. Yokoyama, T. D. Dao, M.-G. Sun, P. S. Pankin, I. V. Timofeev, T. Nagao, and K.-P. Chen, *ACS Photonics* **4**, 2212 (2017).
- 48 O. Gazzano, S. Michaelis de Vasconcellos, K. Gauthron, C. Symonds, P. Voisin, J. Bellessa, A. Lemaitre, and P. Senellart, *Appl. Phys. Lett.* **100**, 232111 (2012).
- 49 C. Symonds, A. Lemaitre, P. Senellart, M. H. Jomaa, S. Aberra Guebrou, E. Homeyer, G. Brucoli, and J. Bellessa, *Appl. Phys. Lett.* **100**, 121122 (2012).
- 50 R. Brückner, A. A. Zakhidov, R. Scholz, M. Sudzius, S. I. Hintschich, H. Fröb, V. G. Lyssenko, and K. Leo, *Nat. Photonics* **6**, 322 (2012).
- 51 C. Symonds, G. Lheureux, J. P. Hugonin, J. J. Greffet, J. Laverdant, G. Brucoli, A. Lemaitre, P. Senellart, and J. Bellessa, *Nano Lett.* **13**, 3179 (2013).
- 52 V. A. Belyakov and S. V. Semenov, *J. Exp. Theor. Phys.* **109**, 687 (2009).

- <sup>53</sup>G. Lheureux, S. Azzini, C. Symonds, P. Senellart, A. Lemaitre, C. Sauvan, J.-P. Hugonin, J.-J. Greffet, and J. Bellessa, *ACS Photonics* **2**, 842 (2015).
- <sup>54</sup>M. Ozaki, M. Kasano, T. Kitasho, D. Ganzke, W. Haase, and K. Yoshino, *Adv. Mater.* **15**, 974 (2003).
- <sup>55</sup>M. I. Barnik, L. M. Blinov, V. V. Lazarev, S. P. Palto, B. A. Umanskii, and N. M. Shtykov, *J. Appl. Phys.* **103**, 123113 (2008).
- <sup>56</sup>S. M. Morris, A. D. Ford, M. N. Pivnenko, and H. J. Coles, *J. Appl. Phys.* **97**, 023103 (2004).
- <sup>57</sup>A. Chanishvili, G. Chilaya, G. Petriashvili, R. Barberi, R. Bartolino, G. Cipparrone, A. Mazzulla, R. Gimenez, L. Oriol, and M. Pinol, *Appl. Phys. Lett.* **86**, 051107 (2005).
- <sup>58</sup>H. Finkelmann, S. T. Kim, A. Muñoz, P. Palffy-Muhoray, and B. Taheri, *Adv. Mater.* **13**, 1069 (2001).
- <sup>59</sup>M. O. Ko, S.-J. Kim, J.-H. Kim, B. W. Lee, and M. Y. Jeon, *J. Opt. Soc. Korea* **19**, 346 (2015).
- <sup>60</sup>H. J. Lee, S.-J. Kim, M. O. Ko, J.-H. Kim, and M. Y. Jeon, *Opt. Commun.* **410**, 637 (2018).
- <sup>61</sup>L. M. Blinov, G. Cipparrone, A. Mazzulla, P. Pagliusi, V. V. Lazarev, and S. P. Palto, *Appl. Phys. Lett.* **90**, 131103 (2007).
- <sup>62</sup>Z. Wang, A. K. Mallik, F. Wei, Z. Wang, A. Rout, Q. Wu, and Y. Semenova, *Opt. Express* **29**, 23569 (2021).
- <sup>63</sup>R.-P. Pan, Y.-P. Lan, C.-Y. Chen, and C.-L. Pan, *Mol. Cryst. Liq. Cryst.* **413**, 499 (2004).
- <sup>64</sup>L. M. Blinov and R. Bartolino, *Liquid Crystal Microlasers* (Transworld Research Network, Kerala, 2010).
- <sup>65</sup>V. I. Kopp, Z.-Q. Zhang, and A. Z. Genack, *Prog. Quantum Electron.* **27**, 369 (2003).
- <sup>66</sup>L. M. Blinov, G. Cipparrone, P. Pagliusi, V. V. Lazarev, and S. P. Palto, *Appl. Phys. Lett.* **89**, 031114 (2006).
- <sup>67</sup>S. Palto, N. Shtykov, B. Umansky, M. Barnik, and L. Blinov, *Opto-Electron. Rev.* **14**, 323–328 (2006).
- <sup>68</sup>J. Ortega, C. L. Folcia, G. Sanz-Enguita, I. Aramburu, and J. Etxebarria, *Opt. Express* **23**, 27369 (2015).
- <sup>69</sup>H. Kogelnik and C. V. Shank, *J. Appl. Phys.* **43**, 2327 (1972).
- <sup>70</sup>K. W. Yoon and N. Y. Ha, *Opt. Express* **24**, 516 (2016).
- <sup>71</sup>I. Nys, J. Beeckman, and K. Neyts, *J. Opt. Soc. Am. B* **31**, 1516 (2014).
- <sup>72</sup>H. Kogelnik, *Bell Syst. Tech. J.* **48**, 2909 (1969).
- <sup>73</sup>A. Yariv and P. Yeh, *Optical Waves in Crystals: Propagation and Control of Laser Radiation* (John Wiley & Sons, Hoboken, 2002).
- <sup>74</sup>C.-Y. Chang, Y.-H. Chen, Y.-L. Tsai, H.-C. Kuo, and K.-P. Chen, *IEEE J. Sel. Top. Quantum Electron.* **21**, 262 (2015).
- <sup>75</sup>A. D. Rakić, A. B. Djurišić, J. M. Elazar, and M. L. Majewski, *Appl. Opt.* **37**, 5271 (1998).
- <sup>76</sup>P. García Parejo and A. Álvarez-Herrero, *Opt. Mater. Express* **9**, 2681 (2019).
- <sup>77</sup>N. M. Shtykov and S. P. Palto, *J. Exp. Theor. Phys.* **118**, 822 (2014).